



Contents lists available at ScienceDirect

Arabian Journal of Chemistry

journal homepage: www.ksu.edu.sa

Preparation and performance of FeCo bimetallic organic frameworks with super adsorption and excellent peroxymonosulfate activation for tetracycline removal

Shuangfei Zhang, Ziru Shao, Deyong Wu*

Hubei Key Laboratory of Biologic Resources Protection and Utilization, School of Chemical and Environmental Engineering, Hubei Minzu University, Enshi, Hubei Province 445000, China

ARTICLE INFO

Keywords:
Bimetallic
Adsorption
Peroxymonosulfate
Mechanism

ABSTRACT

As bifunctional materials for adsorption and peroxymonosulfate (PMS) activation, iron – cobalt bimetallic organic frameworks (FeCo – MOF) were successfully fabricated via a facile method at room temperature, and characterized by XRD, SEM, TEM, XPS, TGA, BET and FTIR. Due to the high specific surface area and electrostatic interaction, FeCo – MOF showed excellent adsorption capacity. 30 mg of FeCo – MOF can adsorb 87.5 % of tetracycline (TC) in a 100 mL aqueous solution (70 mg/L). The adsorption data are well fitted by the Langmuir model and pseudo – second – order adsorption kinetics, indicating the TC capture probably was monolayer molecular adsorption and chemisorption. Meanwhile, FeCo – MOF/PMS had the outstanding catalytic activity for TC degradation via PMS activation. 10 mg of FeCo – MOF can remove 91 % of TC within 5 min in a 100 mL aqueous solution (20 mg/L) with PMS (0.1 mmol·L⁻¹). Quenching experiments showed that •OH, SO₄^{•-}, O₂^{•-} and ¹O₂ all participate in the TC degradation. The effects of PMS concentration, pH value, reaction temperature on TC degradation were investigated. Although the coexisting inorganic anions and small molecule acids inhibited the catalytic performance of FeCo – MOF/PMS, the TC removal rates were still greater than 80 %, indicating the FeCo – MOF/PMS system has a strong anti – interference ability to complex water environments. In addition, the complete degradation of various pollutants, including TC, methylene orange (MO) and methyl blue (MB), and TC degradation in different water bodies confirmed the wide applicability of the FeCo – MOF/PMS system.

1. Introduction

In recent years, with the rapid development of industry, water pollution has become more and more serious, and then been highly concerned. Therefore, the safe and effective treatment of water pollutants has become a hot topic of research (El-Aswar et al., 2022); (Ghorbani et al., 2023) ; (Samy et al., 2023) . Tetracyclines (TCs) are a group of broad-spectrum antibiotics having vast human, veterinary, and aquaculture applications. The continuous release of TCs residues into the environment and the inadequate removal through the conventional treatment systems result in its prevalent occurrence in soil, surface water, groundwater, and even in drinking water (Scaria et al., 2021). Among all of the antibiotics, tetracycline (TC) ranks second in production and usage throughout the world and possesses antibacterial activities against a wide range of pathogenic bacteria. Misuse of TC will not

only raise potential risk to ecosystems and human health, but also lead to increased antimicrobial resistance of microorganism. Hence, the removal of TC from water is of importance from the perspective of environmental protection and health (Chen et al., 2021).

Sulfate radical – based advanced oxidation processes (SR – AOPs) have been proved as an efficient and concise way to deal with water pollution (Azizollahi et al., 2023); (Trawiński et al., 2022) ; (Xu et al., 2022) . Sulfate radical (SO₄^{•-}) has higher redox potential and longer half – life than that of hydroxyl radical (•OH) (Wang et al., 2022); (Zhou et al., 2023) . Peroxymonosulfate (PMS), as one kind of the oxidant in SR – AOPs, can be activated by various strategies (Bui et al., 2021); (Yang et al., 2023) ; (Yuan et al., 2021); (Zhang et al., 2023). Among them, heterogeneous transition metal activation systems own some especial advantages, such as simple reaction systems, mild reaction conditions, no additional energy, and the collaboration between loaded

Peer review under responsibility of King Saud University.

* Corresponding author.

E-mail address: wdy001815@126.com (D. Wu).

<https://doi.org/10.1016/j.arabjc.2023.105483>

Received 9 October 2023; Accepted 22 November 2023

Available online 23 November 2023

1878-5352/© 2023 The Authors. Published by Elsevier B.V. on behalf of King Saud University. This is an open access article under the CC BY-NC-ND license (<http://creativecommons.org/licenses/by-nc-nd/4.0/>).

materials and transition metals (ElMetwally et al., 2021); (Qin et al., 2018); (Huang et al., 2023). Due to the adjustable structure and porous size, high surface area, more metal active sites, metal – organic frames (MOFs) always be used to activate persulfate (Masoomi et al., 2019); (Shi et al., 2019); (Xia et al., 2021). Numerous studies have shown that the reaction mechanism of $\text{SO}_4^{\bullet -}$ and organic matter is mainly through three reaction mechanisms: electron transfer, hydrogen extraction and addition. MOFs not only provides the active site but also improves the electron transfer, and thus efficiently activates the PMS to produce active oxides (Zhong et al., 2022).

Bimetallic MOFs retain most of the advantages of monomeric MOFs, and have higher catalytic activity and stability than monomeric MOFs (Chen et al., 2020); (Liu et al., 2022); (Luo et al., 2023); (Sanati et al., 2021); (Sanati et al., 2022). In this work, We synthesized iron – cobalt bimetallic organic frameworks (FeCo – MOF) according to a modified simple and safe synthesis method (Ge et al., 2021). DMF was used as organic solvent, 1,4 – benzenedicarboxylic acid as organic linker, iron and cobalt salt as metal source, and a small amount of triethylamine (TEA) as structural control agent. The mixture of a small amount of water and ethanol to prevent the agglomeration of the ideal material structure. Meanwhile, because of the high surface area, MOFs always be used as an adsorbent to remove various organic pollutants (Zhang et al., 2023). In our study, it is found that the adsorption of FeCo – MOF for tetracycline hydrochloride (TC) is more consistent with the pseudo – second – order kinetic model and belongs to chemical adsorption. The adsorption thermodynamic study showed that the adsorption process is spontaneous and belongs to the Freundlich model (Jiang et al., 2023).

The prepared FeCo – MOF were systematically characterized by TGA, SEM, HRTEM, XRD, FTIR, BET and XPS. The catalytic ability of FeCo – MOF for PMS activation was evaluated through the TC degradation. The results showed that the FeCo – MOF/PMS system was better than the Fe – MOF/PMS and Co – MOF/PMS for the TC degradation. The influencing factors were also investigated, such as the reaction temperatures, initial pH value, PMS concentrations, catalyst dosage, and the presence of various inorganic anions. Furthermore, the applicability and stability of the FeCo – MOF/PMS system were also evaluated. In addition, the generated reactive oxygen species (ROS) in the FeCo – MOF/PMS system were verified by the quenching experiment, and the reaction mechanisms of the FeCo – MOF/PMS system for TC degradation was illustrated.

2. Experimental part

2.1. Reagents and materials

The chemicals in this study were purchased in analytical grade and used without any additional purification, the deionized water used in this research was purified by Millipore Milli – Q system. $\text{FeCl}_3 \cdot 6\text{H}_2\text{O}$, $\text{Co}(\text{NO}_3)_2 \cdot 6\text{H}_2\text{O}$, triethylamine (TEA), tert – butanol (TBA), isopropyl alcohol (IPA), furfurfural (FFA), sodium chloride (NaCl) and sodium sulfate (Na_2SO_4), tetracycline hydrochloride (TC), methyl orange (MO) and submethyl blue (MB) were purchased from MacLean Biochemical Ltd. (Shanghai, China). Potassium persulfate (PMS) and N, N – dimethylformamide (DMF) were purchased from Aladdin Biochemical Technology Co., Ltd. (Shanghai, China). Para – phthalic acid (PTA), ethanol (EtOH), methanol (MeOH) and ascorbic acid (AA), sodium carbonate (Na_2CO_3) and sodium bicarbonate (NaHCO_3) were purchased from Sinopharm Chemical Reagents Co., Ltd. Sodium nitrate (NaNO_3) and sodium dihydrogen phosphate (NaH_2PO_4) were obtained from Tianjin Fuchen Chemical Reagent Factory.

2.2. Synthesis of FeCo – MOF, Fe – MOF, Co – MOF

Firstly, 0.18 g of $\text{Co}(\text{NO}_3)_2 \cdot 6\text{H}_2\text{O}$, 0.36 g of $\text{FeCl}_3 \cdot 6\text{H}_2\text{O}$, 0.24 g terephthalic acid (2,4 – BDC) were mixed in 100 mL of DMF solution under stirring in a conical flask at room temperature for one hour, and the

mixture was sonicated for another 1 h. Next, 5 mL of deionized water, 10 mL of ethanol and 10 mL of triethylamine (TEA) were added, and the mixture was sequentially stirred at room temperature for 12 h. Then, the precipitate was collected by centrifugation, washed with ethanol for three times, and then stirred in ethanol for 6 h. Products were finally collected by centrifugation and vacuum – dried at 50°C overnight to obtain the desired finished product. The synthesis process of FeCo – MOF is illustrated (Fig. 1). As control samples, monometallic MOFs were prepared by the same method as described above, using the same total metal molar concentration as bimetallic-based MOFs, but without adding $\text{Co}(\text{NO}_3)_2 \cdot 6\text{H}_2\text{O}$ or $\text{FeCl}_3 \cdot 6\text{H}_2\text{O}$, which were defined as (Fe – MOF or Co – MOF), respectively.

2.3. Material characterization

X – ray powder diffraction (XRD) pattern of samples were recorded on a powder X – ray diffractometer (D/max – 2200/PC, Rigaku Corporation, Japan) with Cu K α radiation, operating at 40 kV and 30 mA, where $\lambda = 0.15418$ nm for the Cu K α line. XPS experiments were carried out on a RBD upgraded PHI – 5000C ESCA system (Perkin – Elmer, USA), the shift of the binding energy due to relative surface charging was corrected using the C 1 s level at 284.6 eV as an internal standard. The structure and morphology of the coatings were investigated by the field emission scanning electron microscopy (FESEM, FEI SIRION 200, FEI, USA) and Transmission Electron Microscope (TEM, JEM – 100CX, JEOL, Japan). The functional groups in FeCo – MOF were identified by Fourier Transform Infrared Spectroscopy (FT – IR, FTS3000FX, DIGILAB, USA). The surface area and pore diameter were determined by a Micromeritics surface area analyzer at a liquid N_2 temperature of 77 K. Thermogravimetric analysis (TGA) was conducted in the temperature range of 30–800 °C at heating rate of 10 °C min^{-1} using PerkinElmer TGA/Pyris 1 analyzer.

2.4. Experimental procedures

2.4.1. Adsorption experiments

All adsorption experiments were performed in a 200 mL conical flask placed in a thermostatic water bath oscillator. The adsorption properties of FeCo – MOF was evaluated by the amount of adsorption of TC. Place 0.03 g of adsorbent in 100 mL of TC (30, 40, 50, 60, 70 mg/L) at 298 K under stirring with speed of 200 rpm. Under continuous stirring, a certain amount of suspension was taken at interval time, and immediately filtrated by a 0.22 mm hydropolysulfone filter to measure the concentration by a UV – vis spectrometer. The similar processes were adopted at different temperatures (298 K, 308 K, 318 K, 328 K) to measure the equilibrium concentration and analyze the adsorption thermodynamics.

2.4.2. Catalytic experiments

The catalytic performance of FeCo – MOF was evaluated by activating PMS to degrade TC. Typically, 0.01 g of the prepared catalyst was placed into 100 mL of TC (20 mg/L), and the mixture were stirred at room temperature for 10 min to form a uniformly dispersed phase. Then, 0.1 mL of PMS solution (1 mol/L) was added to the above suspension to allow PMS activation to generate active species for TC degradation. Under stirring, a certain amount of suspension was extracted with a disposable syringe at a specified time interval (5 min), filtered through a 0.22 μm drainage polyether sulfone filter membrane, and measured its concentration at a wavelength of 357 nm using a UV – visible spectrophotometer. In order to assess the extensive degradability of organic pollutants by the FeCo – MOF/PMS system, the degradation of MB and MO was also understood under the same conditions, and the concentrations were measured at 664 nm and 464 nm using a UV – visible spectrophotometer.

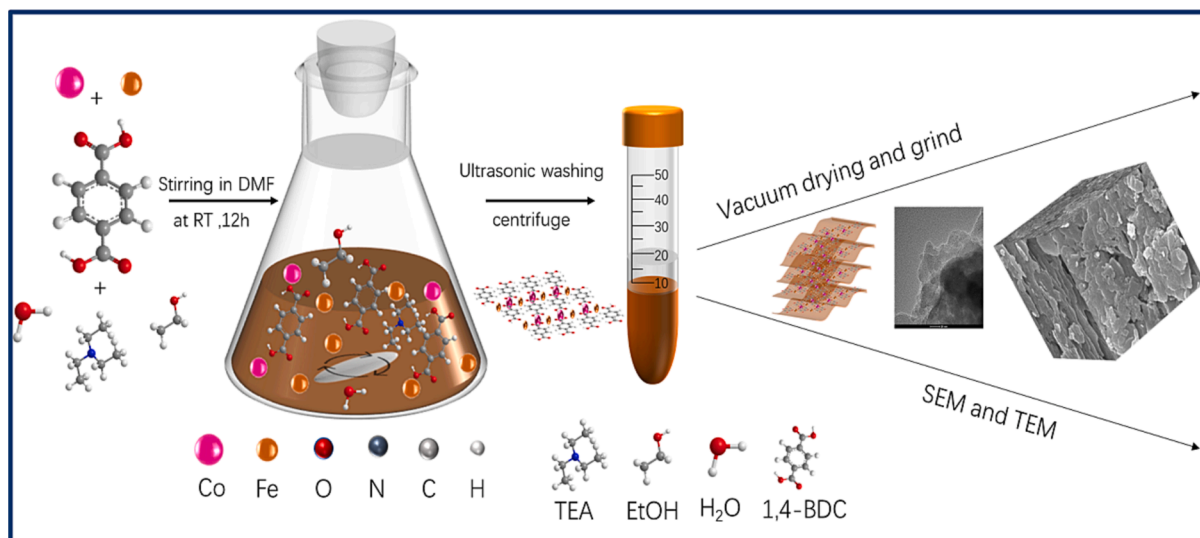


Fig. 1. Graphic procedure of FeCo – MOF synthesis.

3. Results and discussion

3.1. Material characterization

The crystal structures of asprepared Fe – MOF, Co – MOF and FeCo

– MOF were analyzed by XRD patterns (Fig. 2a). Co – MOF has very distinct diffraction peaks at 8.28° , 15.24° , 17.14° , which can be assigned to the (200), (201), and (400) planes of the layered triad structure (Zhao et al., 2017). However, no obvious diffraction peak was detected for Fe – MOF, which indicates its poor crystallinity. Moreover the FeCo

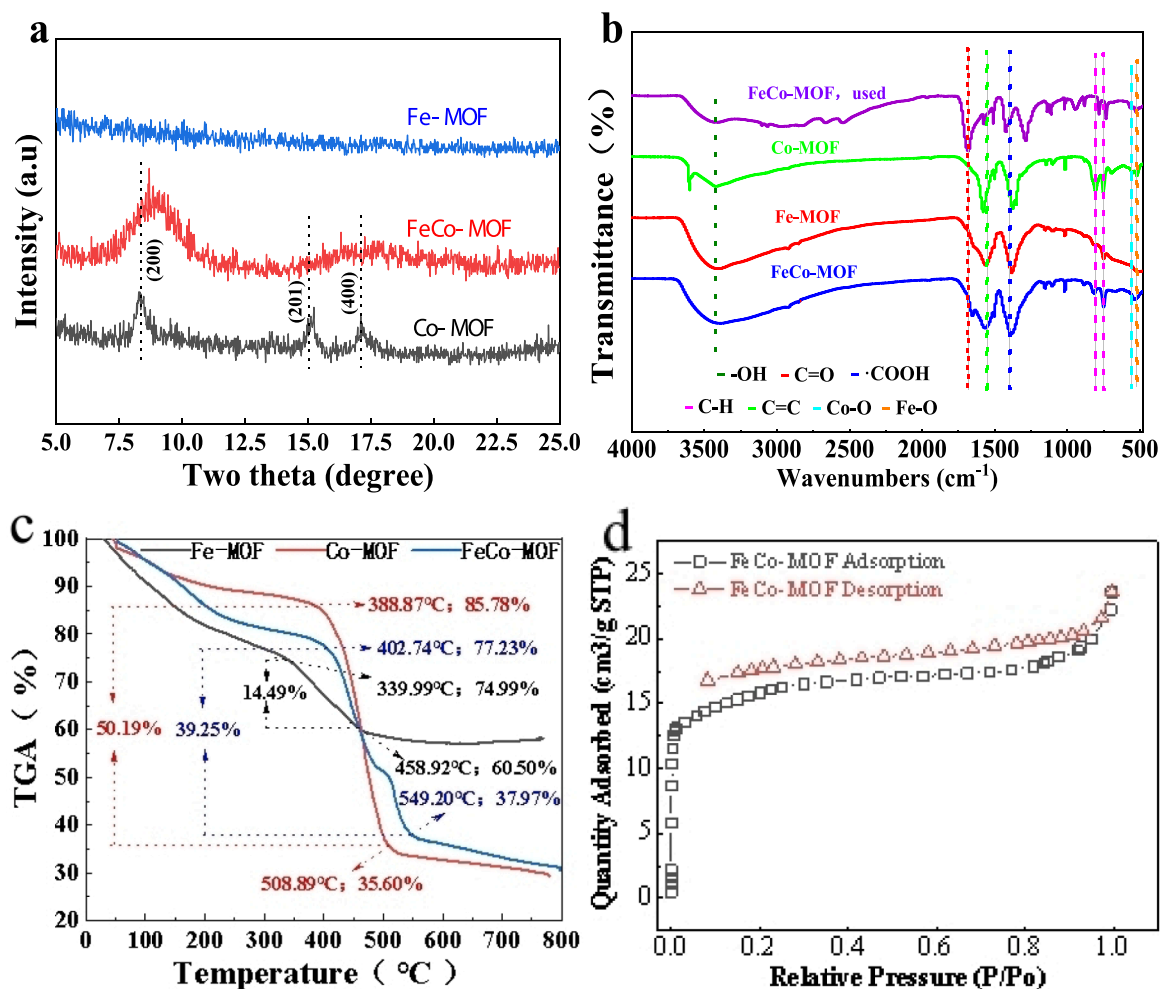


Fig. 2. (a) XRD patterns, (b) FT – IR spectra and (c) TGA files of Fe – MOF, Co – MOF and FeCo – MOF. (d) N₂ adsorption – desorption isotherm of FeCo – MOF.

– MOF only showed a significant diffraction peak at 8.7°, corresponding to the (200) crystal surface, indicating the introduction of Fe affects the structure of Co – MOF. To insight on the surface chemistry characteristics of the prepared materials, the FTIR spectroscopy was utilized to analyze the functional groups in Fe – MOF, Co – MOF, FeCo – MOF and FeCo – MOF collected after TC degradation (Fig. 2b). The absorption peaks at around 755 cm⁻¹ and 818 cm⁻¹ are due to the bending vibration of the C – H bond on the benzene ring of the organic ligand (Li et al., 2021); (Zhang et al., 2015). Note that symmetrical vibration peaks of – COOH appear at positions around 1390 cm⁻¹, indicating that the organic ligand in the prepared material is p – phthalic acid (Gong et al., 2017). The peaks at 1570 and 3430 cm⁻¹ respectively corresponded to the C = C stretching vibrations of the aromatic ring and –OH groups (Liu et al., 2017). The stretching vibrations of C = O lead to adsorption peaks at 1660 cm⁻¹. The absorption peaks at low frequencies of less than 600 cm⁻¹ were attributed to metal – oxo bond (M – O) vibrations. Thus, the peaks generated near 558 cm⁻¹ represent the stretching vibration of the Co – O bond from Co – MOF and FeCo – MOF. However, the peaks generated near 532 cm⁻¹ represent the stretching vibration of the Fe – O bond from Fe – MOF and FeCo – MOF, which demonstrated the successful fabrication of FeCo – based bimetallic organic frameworks (Banerjee et al., 2012).

The TGA profiles of Fe – MOF, Co – MOF, and FeCo – MOF materials were shown in Fig. 2c. When Fe – MOF rises from room temperature to about 340°C, the weight decreases to 74.99%, which should be caused by the evaporation loss of water in Fe – MOF. Then, between 340 °C to 459 °C, the mass loss of Fe – MOF was 14.49%, which may be caused by the destruction of the structure and the carbonization of organic matter. While the quality of Fe – MOF barely unchanged between 459 °C and 800 °C. When Co – MOF rises from room temperature to about 389°C, the loss of water evaporation resulted in mass reduction to 85.78%. Then, between 389°C and 509°C, a massive mass loss of the Co – MOF occurs due to the carbonization of the organic matter, The mass loss was 50.19%. There mass of the Co – MOF was also very little change between 509 °C and 800 °C. When FeCo – MOF rises from room temperature to about 403 °C, the loss of water evaporation causes the mass reduction to 77.23%. Then, between 403 °C and 549 °C, the mass loss of FeCo – MOF occurred due to the carbonization of organic matter occurred, with a mass loss of 39.25%. However, the FeCo – MOF quality barely unchanged between 549 °C and 800 °C. From the weight loss of the three materials, it is found that Fe – MOF loses the least weight, followed by FeCo – MOF, while Co – MOF has the most weight loss. The most direct reason for this is the spatial structure of the three materials. N₂ adsorption – desorption isotherm of FeCo – MOF was measured (Fig. 2d). It appears the type I isotherm, which is a typical feature of microporous materials. The BET surface area of FeCo – MOF was approximately 57.77 m² · g⁻¹. The pore diameter distribution curves of FeCo – MOF was displayed in Fig.S1.

The microstructure and morphology of the prepared MOFs were characterized by SEM and TEM. Fe – MOF has a tightly packed large structure and no complex spatial structure on the surface (Fig.S2). Conversely, Co – MOF has a distinct sheet – stacked structure (Fig.S3), indicating its characteristic of high crystallinity. As shown in Fig.S4, the apparent structure of FeCo – MOF was formed by the agglomerated block structure and the lamellar stacking structure. The TEM images showed a layered structure of the FeCo – MOF with a uniform distribution (Fig.S5). The EDS mapping of FeCo – MOF showed a uniform distribution of C, O, Fe and Co elements (Fig.S6).

3.2. Adsorptive performances of FeCo – MOF

3.2.1. TC adsorption

The standard curve between concentration and absorbance of TC was showed in Fig.S7. The concentration of TC can be calculated based on the standard curve. The adsorption capacity (q_t, mg · g⁻¹) and removal efficiency (%) of TC by the FeCo – MOF can be calculated based

formulas (1—3) (Jiang et al., 2023):

$$q_t = \frac{(C_0 - C_t)V}{W} \quad (1)$$

$$q_e = \frac{(C_0 - C_e)V}{W} \quad (2)$$

$$\text{Removal efficiency}(\%) = \frac{(C_0 - C_e) \times 100}{C_0} \quad (3)$$

where C₀, C_e and C_t (mg · L⁻¹) respectively represent the Initial concentration, concentration at equilibrium, and concentration at a certain time (min) of TC; q_t and q_e (mg · g⁻¹) denotes the represents adsorbance for a certain time and at adsorption equilibrium, respectively; V (L) and W (mg) are the volume of TC solution and mass of adsorbent, respectively.

As shown in Fig. 3a, The initial concentration of TC is different, and the amount of adsorbent adsorption to TC is different. The greater the concentration of TC, the more TC is adsorbed, and the faster the adsorption rate. In addition, the times for reaching the adsorption equilibrium at different original TC concentrations were different. It needed longer time to reach equilibrium if the original concentration of TC was higher. This phenomenon is attributed to the lack of adsorption sites on the FeCo – MOF surface to capture more TC (Jiang et al., 2023). In the initial concentration of TC solution, only a small part of TC molecules can be quickly captured on the surface, while most of them enter the structure of FeCo – MOF by intramolecular diffusion. Also shown in Fig. 3b, when the concentration of TC increased from 30 mg/L to 70 mg/L, the adsorption amount (q_e) at adsorption equilibrium increased steadily, and q_e increased from 99.8 mg · g⁻¹ to 198.8 mg · g⁻¹. Conversely, the removal rate of TC showed a gradual decline, decreasing from 99% at the beginning to 87.5%. This phenomenon may also be attributed to the larger the concentration of TC, the more the final adsorption amount, but the limited FeCo – MOF surface adsorption site is not enough to capture more TC, resulting in a decrease in the removal rate (Liu et al., 2014).

3.2.2. Adsorption kinetics

The adsorption equilibrium data of TC on FeCo – MOF were fitted by two extensively used kinetic models, i.e., pseudo – first – order kinetics, pseudo – second – order kinetics models. The above mentioned kinetics model equations are respectively expressed as follows (Al-Mhyawi et al., 2023); (Valadi et al., 2022); (Vinayagam et al., 2023):

The pseudo – first – order kinetics model:

$$\ln\left(\frac{q_e}{q_e - q_t}\right) = \frac{k_1 t}{2.303} \quad (4)$$

The pseudo – second – order kinetics model:

$$\frac{t}{q_t} = \frac{1}{k_2 q_e^2} + \frac{t}{q_e} \quad (5)$$

where k₁ (min⁻¹) and k₂ (g/mg min⁻¹) severally denote the rate constants of pseudo – first – order and pseudo – second – order equations.

The circumstantial adsorption behavior of FeCo – MOF was further investigated. Two pseudo kinetic models were fitted to obtain the regression curves and further used for calculating relevant parameters (Fig. 4). As a result, the regression correlation coefficients of non – linear pseudo – second – order kinetic model (R² > 0.97) (Fig. 4b) were evidently larger than that of the non – linear pseudo – first – order kinetic model (R² < 0.97) (Fig. 4d) for all TC concentrations. However, the R² values obtained by the two pseudo kinetic models are not much different, and the quasi – second order is all larger than the quasi – first – order dynamics except at the TC concentration of 60 mg/L. This is consistent with the nonlinear fit. Notably, the pseudo – second – order kinetic model was much fit for depicting the adsorption of TC on FeCo –

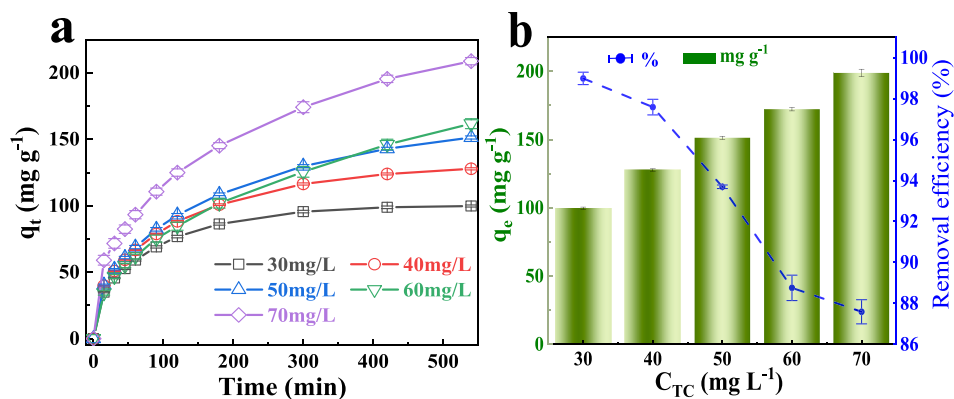


Fig. 3. (a) The amount of adsorption (q_t) different concentrations of TC varies over time. (b) The adsorption amount (q_e) of TC at the adsorption equilibrium and the removal rate (Re) of TC change with the change of TC concentration.

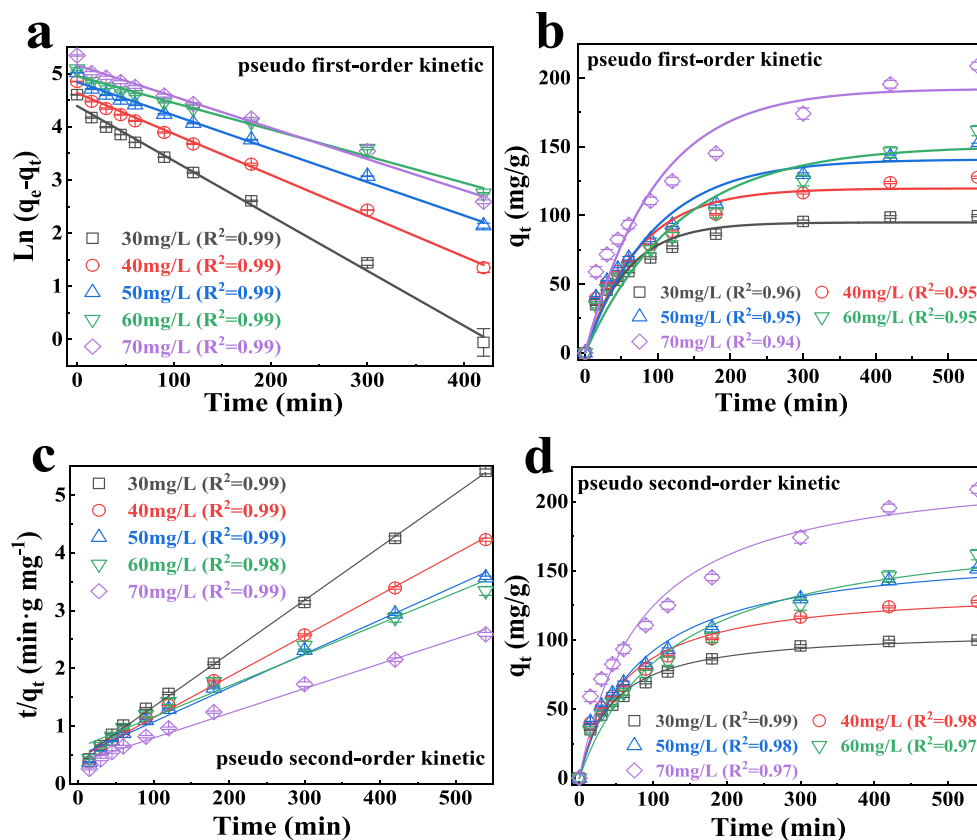


Fig. 4. Plots of linear and non – linear pseudo first – order kinetic (a, b), pseudo second – order kinetic (c, d).

MOF, implying that the chemisorption involved electron exchange, transfer and sharing was the main adsorption rate controlling step (Liu et al., 2014). Meanwhile, the values of q_e increasingly aggrandized with the rising of original TC concentrations. While the rate constants (k_2 values) decreased as the original TC concentrations increased. This observation could be attributing to the competition for the adsorption sites might be high at larger original TC concentrations, leading to a relatively low rate constant.

3.2.3. Adsorption isotherm

The adsorption isotherms from different initial TC concentration at various temperature conditions (298, 308, 318 and 328 K) were performed. The linear and non – linear Langmuir and Freundlich models were respectively fitted based on the equilibrium data (Fig. 5). The fitted

correlation coefficients got from linear and non – linear Freundlich isotherm models were all above 0.93. The corresponding correlation coefficients got from Langmuir isotherm models were almost above 0.95. The results indicated that the Langmuir model was more suitable for describing current adsorption behavior. Thus, the Langmuir isotherm model could better depicted the current adsorption process, indicating the TC capture probably was monolayer molecular adsorption, and chemisorption.

The expression for both models are as follows (Habimana et al., 2016); (Li et al., 2013) :

Langmuir model:

$$\frac{c_e}{q_e} = \frac{c_e}{q_{\max}} + \frac{1}{q_{\max} \cdot k_L} \quad (6)$$

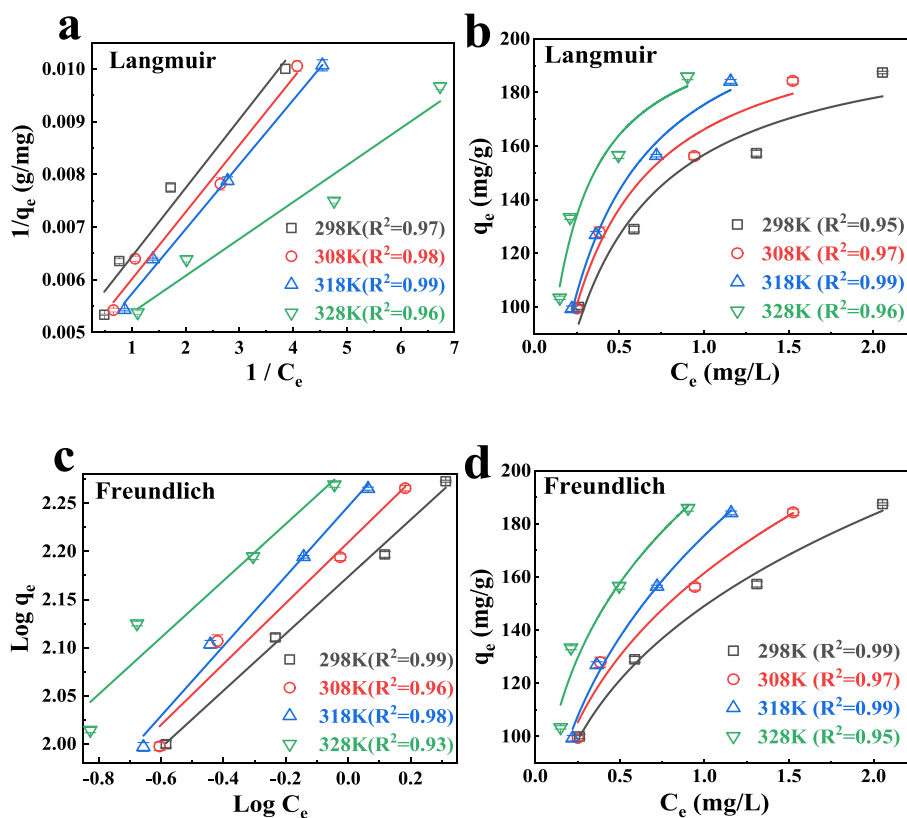


Fig. 5. Plots of linear and non – linear Langmuir model (a, b), Freundlich model (c, d).

Freundlich model:

$$\text{Log } q_e = \text{Log } k_F + \frac{1}{n} \text{Log } C_e \quad (7)$$

Where C_e is the concentration at adsorption equilibrium (mg/L), q_{\max} is the maximum adsorption amount (mg/g), k_L is langmuir constant (L/mg) indicates the adsorption strength; q_e is the adsorption amount at adsorption equilibrium, k_F is Freundlich constant ($\text{mg}^{(n+1)}/\text{g}/\text{L}^n$), indicates the adsorption capacity, n is the adsorption strength.

The constant R_L can reflect the essential characteristics of the langmuir model, expressed as (Liu et al., 2014):

$$R_L = \frac{1}{1 + C_0 K_L} \quad (8)$$

Where C_0 is the initial concentration (mg/L) and k_L is the langmuir constant. When $R_L = 0$, adsorption is irreversible; when $0 < R_L < 1$, adsorption is preferred; when $R_L = 1$, linear adsorption; when $R_L > 1$, adsorption is unfavorable.

The current R_L values between 0.139 and 0.069 in the concentration scope from 30 to 60 mg/L, revealing favorable capture in current adsorption system. It is worth noting that the increases of the original TC concentration and the reaction temperature decreased the R_L values correspondingly, indicating that the high concentration of TC and the increased temperature are conducive to adsorption.

3.2.4. Adsorption thermodynamics

For deeply understanding of the capture behavior, the thermodynamic experiments of adsorption of TC by FeCo – MOF were carried out from 298 to 328 K. The adsorption isotherm curves of non – linear Langmuir model were first fitted to obtain the Langmuir isotherm constants (K_L , L/mg). Results indicated that the capture capacities of TC in the FeCo – MOF gradually increased with the increase of temperature (Fig. 5b), which may be ascribed to the increased mobility of TC

molecules with increasing temperature. Subsequently, Thermodynamic analysis was carried out to further explain the influence of temperature on TC capture. Based on adsorption isotherms results, the thermodynamic parameters such as enthalpy change (ΔH , KJ mol^{-1}), Gibbs free energy change (ΔG , KJ mol^{-1}), and entropy change (ΔS , KJ mol^{-1}) were calculated as the following formulas (Chen et al., 2022); (Chen et al., 2022); (Khakbaz et al., 2022):

$$k_D = k_L \times q_{\max} \quad (9)$$

$$\Delta G = -RT \times \ln k_D \quad (10)$$

$$\ln k_D = \frac{\Delta S}{R} - \frac{\Delta H}{RT} \quad (11)$$

Where K_D and T (K) are the thermodynamic constant at equilibrium and the absolute temperature accordingly; K_L (L/mg) and q_{\max} (mg/g) respectively denote the Langmuir isotherm constant at various temperatures and the theoretical maximum adsorption capacity.

Further, the thermodynamics curve and thermodynamic parameters were respectively fitted and calculated. Results indicated that the ΔH value was $13.53 \text{ KJ mol}^{-1}$, indicating endothermic property of the current adsorption system. It means that enhancing temperature would be benefit to the boosting of TC uptake. Negative ΔG (-9.051 , -9.386 , -9.857 , and $-10.006 \text{ kJ mol}^{-1}$ at 298, 308, 318 and 328 K, respectively) revealing spontaneous characteristics of adsorption behavior. In addition, positive ΔS ($0.49 \text{ J mol}^{-1}\text{K}^{-1}$) enhanced the randomness at the solid – solution interface during anchoring of TC onto the binding sites of FeCo – MOF.

3.3. Catalytic performance of FeCo – MOF

The catalytic performance of FeCo – MOF was evaluated by the degradation of TC (Fig. 6a). For significant contrast, only 0.1 mM PMS was added, and the degradation efficiency of TC is 26.4 % for 30 min.

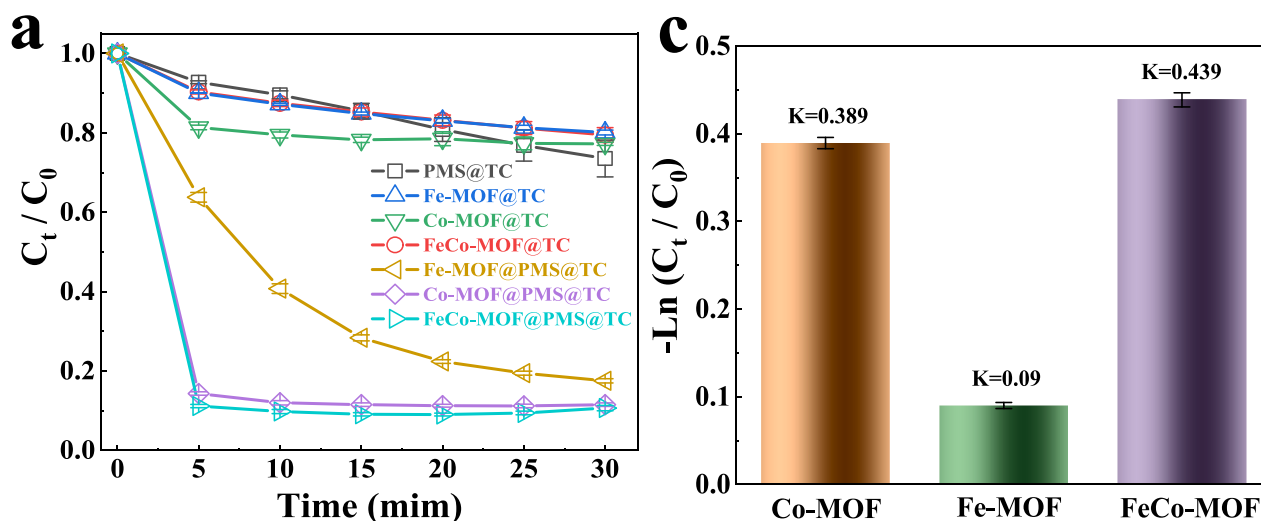


Fig. 6. (a) The degradation of the TC in the different systems, (b) the K values of Fe – MOF/PMS, Co – MOF/PMS and FeCo – MOF/PMS.

This shows that PMS has some self – activation to produce ROS for TC degradation at room temperature, but the effect is not strong. In addition, the removal rates of TC were 19.9 %, 22.8 % and 20.5 % at 30 min by adding Fe – MOF, Co – MOF, FeCo – MOF without PMS, respectively. Exhilaratingly, TC can be quickly degraded when the MOFs and PMS were added into the TC solution simultaneously. The removal rate of TC was 82.5 % for the Fe – MOF/PMS system at 30 min (Fig. S8). Astoundingly, the removal rates of TC were up to 88.5 % and 91.0 % for Co – MOF/PMS and FeCo – MOF/PMS at 5 min, respectively. The apparent rate constant (k) of TC removal was calculated via the pseudo – first – order kinetic model to compare the activation performance (Fig. 6b). The k values were calculated as 0.09, 0.389 and 0.439 min^{-1} for Fe – MOF/PMS, Co – MOF/PMS and FeCo – MOF/PMS, respectively. The result displayed that the bimetallic MOFs have better catalytic activities for PMS activation than that of the monometallic ones. That may be attributed to the existence of synergistic effect between metals.

3.4. Reaction mechanism

To unravel the primary ROS for the TC elimination in FeCo – MOF/

PMS systems, the following scavenging experiments were performed. Ascorbic acid (AA), furfuryl alcohol (FFA), tert – butanol (TBA) and methanol (MeOH), were used as effective radical scavenger to scavenge superoxide radical ($\text{O}_2^{\bullet-}$), singlet oxygen ($^1\text{O}_2$), sulfate radical ($\text{SO}_4^{\bullet-}$), $\text{SO}_4^{\bullet-}$ /hydroxyl radical ($\bullet\text{OH}$), respectively. Besides isopropyl alcohol (IPA) also can trap $\text{SO}_4^{\bullet-}/\bullet\text{OH}$ (Wang et al., 2022); (Zhang et al., 2015). As shown in (Fig. 7a), With the addition of 100 mM TBA, the degradation rate of TC decreased from 91 % to 83 %, and the K value decreased from 0.439 min^{-1} to 0.203 min^{-1} , suggesting the involvement of $\bullet\text{OH}$ in the system. When 100 mM MeOH or IPA was added, the TC degradation rate was reduced to 67 % or 68 %, the K value decreased to 0.121 min^{-1} or 0.119 min^{-1} . This verified the participation of $\bullet\text{OH}$ for TC degradation. However, 5 mM FFA was added, the TC degradation rate was only 31 %, and the K value decreased to 0.036 min^{-1} , when 5 mM AA was added, the TC degradation rate was only 0.02 %, and the K value was only 0.003 min^{-1} (Fig. 7b), indicating that $^1\text{O}_2$ and $\text{O}_2^{\bullet-}$ are the main reactive oxygen species, while $\text{SO}_4^{\bullet-}$ and $\bullet\text{OH}$ played a supporting role. The combination of four reactive oxygen species makes the catalytic degradation effect of the system very significant, which further shows the excellent application prospect of the material.

To unveil the mechanism of electron transfer and conversion

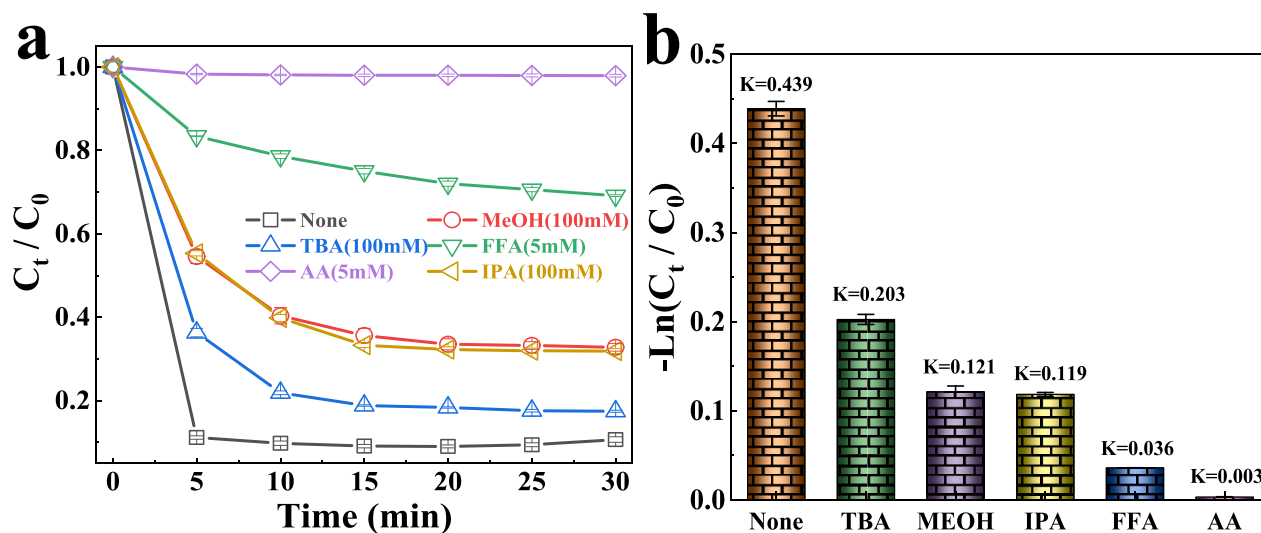


Fig. 7. (a) Effect of free radical capture agent on TC degradation in the FeCo – MOF / PMS system, (b) the corresponding values. Experimental condition: $[\text{TC}]_0 = 20$ mg/L, $[\text{PMS}]_0 = 0.1$ mM, $[\text{catalyst}]_0 = 100$ mg/L, $\text{pH} \approx 6$, $T \approx 298$ K.

between bimetallic sites and PMS during the oxidation reaction, the chemical composition of FeCo – MOF before and after the reaction were analyzed by XPS. As seen in Fig. 8a – b, four peaks for C 1s (284 eV), O 1s (531 eV), Fe 2p (713 eV), and Co 2p (782 eV) were displayed clearly

in the XPS survey spectra (Wang et al., 2016); (Zhao et al., 2022) . However, the peaks of Fe 2p and Co 2p of used FeCo – MOF were not as strong as that of the fresh one. After the oxidation reaction, the Fe²⁺ percentage increased from 74.8 % to 76.5 % while the Fe³⁺ percentage

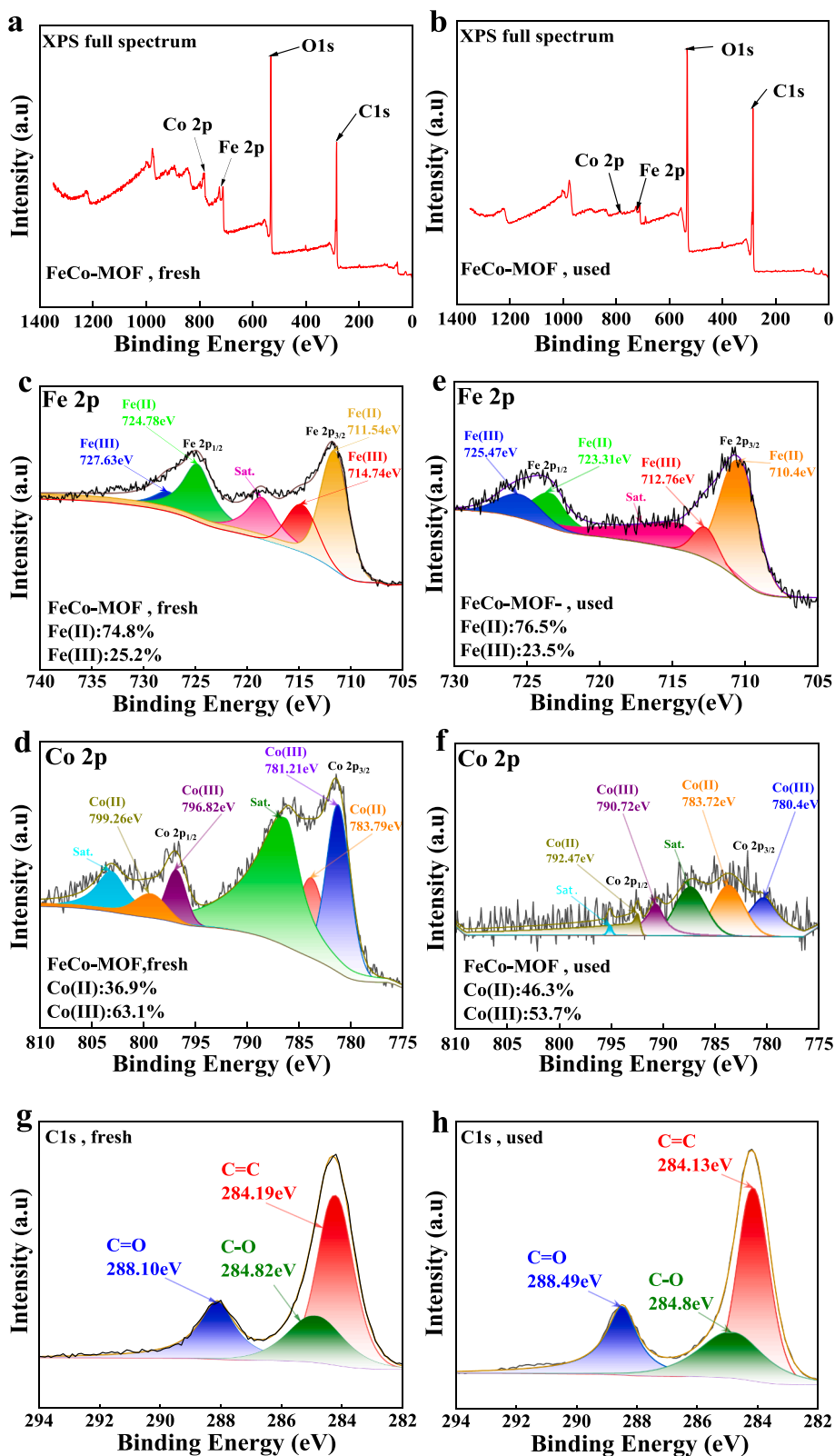
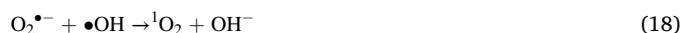
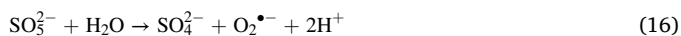


Fig. 8. XPS full spectrum of FeCo – MOF before and after using (a, b). (c) Fe 2p, (d) Co 2p XPS spectra of FeCo – MOF before degradation reaction. (e) Fe 2p, (f) Co 2p spectra of FeCo – MOF after reaction. C 1s XPS spectrum of FeCo – MOF before and after using (g, h).

decreased from 25.2 % to 23.5 % (Fig. 8c – d). Similarly, the Co^{2+} percentage increased from 36.9 % to 46.3 %, while the Co^{3+} percentage decreased from 63.1 % to 53.7 % (Fig. 8e – f). These results verified that the bimetallic Fe and Co sites simultaneously involved in the activation of PMS, and form a continuous rapid redox process between $\text{Co}^{3+}/\text{Co}^{2+}$ and $\text{Fe}^{3+}/\text{Fe}^{2+}$ during the oxidation reaction. Instead, the peak of C1s becomes more pronounced (Fig. 8g – h). This may be the activation of PMS caused by partial carbonization of the metal organic frame. But only the intensity changes, and the position remains the same.

Combined with the above analysis, the mechanisms of the PMS activation and ROS evolution processes were proposed in (Fig. 9.). Firstly, PMS has been adsorbed on the surface of the FeCo – MOF and activated by the reaction between PMS and $\text{Co}^{2+}/\text{Fe}^{2+}$ to generate $\text{SO}_4^{\bullet-}$ via electron transfer (Eq.12–13) (Chen et al., 2018); (Pang et al., 2019); (Yao et al., 2014). The $\bullet\text{OH}$ is generated by the reaction of $\text{SO}_4^{\bullet-}$ with water molecules (Eq.14) (Li et al., 2019). Meanwhile, the PMS and the dissolved oxygen in water both can create $\text{O}_2^{\bullet-}$ (Eq.15–16) (Lou et al., 2017); (Rao et al., 2022); (Wang et al., 2021); (Wang et al., 2017); (Zhu et al., 2022). then the generated $\text{O}_2^{\bullet-}$ was converted to $^1\text{O}_2$ by reacting with H^+ or $\bullet\text{OH}$ (Eq. (17) – 18) (Vinayagam et al., 2023; Wang et al., 2022; Wang et al., 2021; Wang et al., 2016; Wang et al., 2022). Since the redox potential of $\text{HSO}_5^-/\text{SO}_5^{\bullet-}$ (1.10 V) is lower than that of $\text{Co}^{3+}/\text{Co}^{2+}$ (1.84 V), the Co^{3+} can be effectively reduced to Co^{2+} via reaction with HSO_5^- , achieving a continuous cycle between $\text{Co}^{3+}/\text{Co}^{2+}$ (Eq.19). However, the redox potential of $\text{Fe}^{3+}/\text{Fe}^{2+}$ (0.77 V) is more negative than that of $\text{HSO}_5^-/\text{SO}_5^{\bullet-}$ (1.10 V), thus reducing Fe^{3+} by PMS is thermodynamically unfavorable. Alternatively, the redox potential of $\text{O}_2^{\bullet-}/\text{O}_2$ is -0.33 V, which is more feasible to reduce Fe^{3+} than PMS. Therefore, the circulation of $\text{Fe}^{3+}/\text{Fe}^{2+}$ can be realized by $\text{O}_2^{\bullet-}$ (Eq.20). The $\text{SO}_5^{\bullet-}$ can react with itself or $\text{Co}^{2+}/\text{Fe}^{2+}$ to generate $^1\text{O}_2$, which could be another pathway of $^1\text{O}_2$ creation (Eqs.21–23). In addition, the electron transfer between bimetals can effectively accelerate the redox process of $\text{Co}^{3+}/\text{Co}^{2+}$ and $\text{Fe}^{3+}/\text{Fe}^{2+}$, thereby promoting the formation of ROS (Eq.24). Finally, the organic contaminants were decomposed by ROS (Eq. (25).



3.5. Effects of the experimental conditions

3.5.1. The effect of temperature

In order to explore the effect of temperature on the FeCo – MOF/PMS system, TC degradation was performed at different temperatures (25°C, 35°C, 45°C, 55°C). As shown in (Fig. 10a), most TC can be degraded at 5 min at the different temperatures. The higher the temperature, the degradation rate is slightly increased. The degradation rates of TC were 88.4 %, 90.5 %, 91.4 % and 92.9 % at 25°C, 35°C, 45°C and 55°C, respectively. The k values calculated by the pseudo – first – order kinetic model were 0.439, 0.479, 0.472, and 0.502 min^{-1} at 25°C, 35°C, 45°C and 55°C, respectively (Fig. 10b). In fact, PMS can be activated by energy, and a higher reaction temperature can supply more energy to promote the decomposition of PMS into more ROS (Duan et al., 2018). In addition, the molecular movement would be accelerated with the increase of temperature, the higher temperature may facilitate the mass transfer process of heterogeneous systems (Asif et al., 2021); (Yu et al., 2022).

3.5.2. The effect of pH value

The effect of pH value on TC elimination was shown in (Fig. 10c – d). When the pH value is between 4 and 8, the degradation efficiency all reached more than 80 %, and the reaction rate constant are 0.253 min^{-1} ,

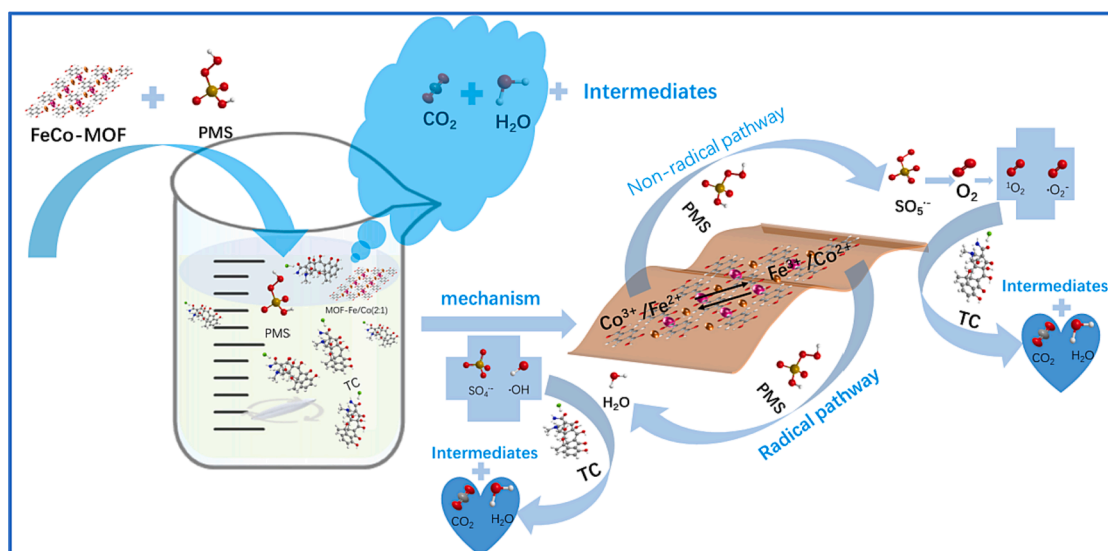


Fig. 9. Schematic illustration of the reaction mechanisms of the FeCo – MOF/PMS system for TC degradation.

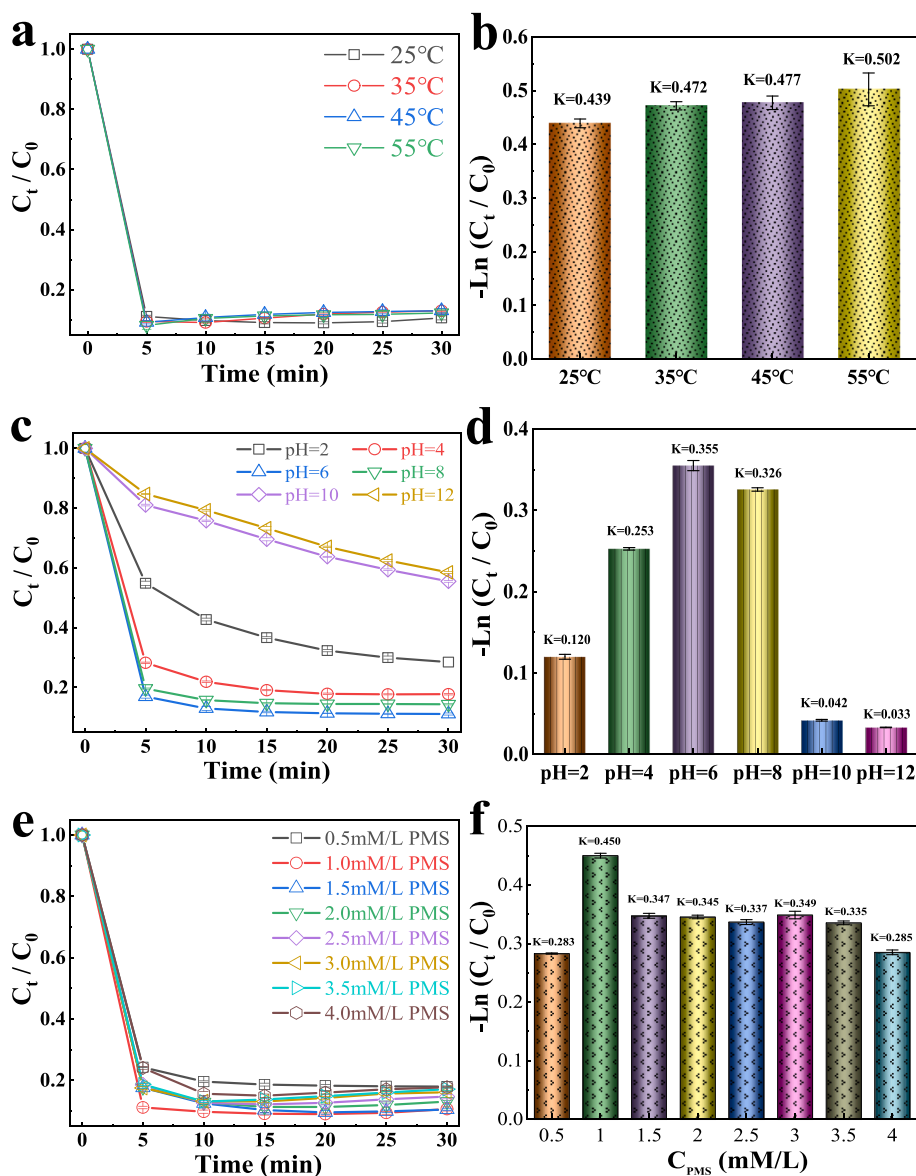


Fig. 10. The effects of temperatures(a), pH values (c) and PMS concentrations (e) on the TC degradation; The K values of TC degradation at different temperatures (b), pH values (d) and PMS concentrations (f). The experimental conditions: $[TC]_0 = 20 \text{ mg/L}$, $[PMS]_0 = 0.1 \text{ mM}$, $[catalyst]_0 = 100 \text{ mg/L}$, $\text{pH} \approx 6$, $T \approx 298 \text{ K}$.

0.355 min^{-1} and 0.326 min^{-1} , respectively. When the pH value was reduced to 2, the removal rate and the reaction rate constant dropped to 71.5 % and 0.120 min^{-1} . This phenomenon was attributed to the stabilizing effect of H^+ on HSO_5^- species (Li et al., 2019); (Lou et al., 2013); (Pan et al., 2020). That is to say, excessive acidic conditions are not conducive to activating PMS to remove pollutants. Increasing the pH value from 8 to 10 strongly inhibited the removal rate. The oxidation efficiency decreased from 85.7 % to 44.5 %, and the k value dropped dramatically to 0.042 min^{-1} . This may be related to two factors. Firstly, cobalt tends to produce hydroxide complexes at pH above 10, resulting in the loss of active metal sites (Lai et al., 2018); (Tan et al., 2022). Secondly, when pH is above 10, SO_5^{2-} will replace HSO_5^- to be the main substance of PMS, which severely hindered the producing of $^1\text{O}_2$ (Liu et al., 2020). Obviously, when the pH value is 12, the oxidation efficiency and K value are even lower, at only 42 % and 0.033 min^{-1} . Therefore, the appropriate pH value of FeCo – MOF/PMS/TC system is about a neutral range of 6 ~ 7, and its effect can be the best. Of course, through experiments, although the pH value is beyond the appropriate range, it still has a good degradation effect.

3.5.3. The effect of PMS concentration

The concentration of catalyst and TC where we fixed this catalytic system is unchanged, and the other experimental conditions are the same as before, the degradation effect of TC was observed by changing the concentration of PMS. As shown in the (Fig. 10e – f), the concentration of PMS was 1 mM/L, the FeCo – MOF/PMS system has the highest catalytic activity. When the concentration of PMS was reduced to 0.5 mM/L, the degradation effect of TC decreases from about 91 % to about 80 %. The k value was also changed from 0.450 min^{-1} to 0.283 min^{-1} . This may be due to the low concentration of PMS leading to fully binding to the active site on the FeCo – MOF surface, which produces a low amount of ROS and fails to adequately degrade the TC. However, when increasing the PMS concentration, the degradation rate of TC did not increase, and its degradation rate constant k value also decreased. Excessive PMS can cause the self – quenching reactions of PMS (Zhao et al., 2021). In addition, as described in Eqs. (26) – (28), excessive PMS will promote the conversion of $\bullet\text{OH}$ and $\text{SO}_4^{\bullet-}$ to $\text{SO}_5^{\bullet-}$ and $\text{HO}_2\bullet$ with lower reactivity (Liu et al., 2021); (Zhao et al., 2021).





3.5.4. The effect of various inorganic anions

The effect of coexisting ions in natural water on the TC oxidation efficiency was studied in the presence of various inorganic ions (SO_4^{2-} , HCO_3^- , CO_3^{2-} , NO_3^- , H_2PO_4^- and Cl^-). The existence of SO_4^{2-} , HCO_3^- , H_2PO_4^- and Cl^- all have nearly negligible effects on the degradation rates (Fig. 11). The main reason is that these inorganic ions can react with $\text{SO}_4^{\bullet-}$ or $\bullet\text{OH}$ to form new radicals with lower oxidation ability (Yan et al., 2021). Take CO_3^{2-} as the sample, 2 mM, CO_3^{2-} was added into the FeCo – MOF/PMS system, the TC removal rate was below 80 %, and the K value was only 0.165 min^{-1} (Fig. S9). As the molar mass of CO_3^{2-} increases, the removal rate of TC also decreases, and the K value continues to decrease. When the molar mass reached 8 mM, the removal rate of TC was only about 70 %, and the k value was only 0.112 min^{-1} . One reason, CO_3^{2-} can react with $\text{SO}_4^{\bullet-}$ or $\bullet\text{OH}$ (Eqs.129,30), leading to the consumption of $\text{SO}_4^{\bullet-}$ or $\bullet\text{OH}$ (Wang and Wang, 2021); (Wang et al., 2022); (Wang and Wang, 2018), and consequentially resulting in lower degradation of TC. Besides, the pH value of the solution should be gradually increased with the addition of CO_3^{2-} , and increasing pH will lead to a decrease in the catalytic activity of FeCo – MOF/PMS system, that has been demonstrated by the experiments about the pH effect on the TC degradation for the FeCo – MOF/PMS system (Fig. 10c). It is gratifying that when all kinds of 2 mM inorganic salts were added to the solution, the removal rate and K value of TC did not decrease significantly (Fig. 11d), which further reflects that the system can show

excellent degradation ability in various complex water environments. HA, as small molecule acids, also inhibited the TC degradation, because HA may compete with PMS for the active sites on the surface of FeCo – MOF, resulting in the reduction of the generated radicals. Delightfully, all the TC removal rates were greater than 80 % and the K value all were greater than 0.25 min^{-1} in the presence of various inorganic ions and HA. These results indicated that the FeCo – MOF/PMS system has a strong anti – interference ability to complex water environments.



3.5.5. The wide applicability

To examine the wide applicability of the system, TC degradation in different water bodies, including deionized water (DW), laboratory tap water (TW) and campus lake water (LW) were explored. As can be seen in (Fig. 12a), the degradation of TC in the deionized water has the best result, followed by the tap water, and the lake water has the worst degradation effect. After 30 min, the degradation rate of TC in deionized water reached 91 %, and that of TC in tap water reached 91.5 %, while the degradation rate of TC in lake water was only 88.5 %, which was slightly lower compared with deionized water and tap water. This may be because the tap water contains a small number of ions that can promote the FeCo – MOF/PMS system, while there are more complex components in the lake water, which affects the degradation of TC. Moreover, as seen from Fig. 12b, the degradation rate constant of TC in deionized water is the largest, reaching 0.439 min^{-1} , the degradation rate constant of TC in tap water is 0.380 min^{-1} , and the degradation rate

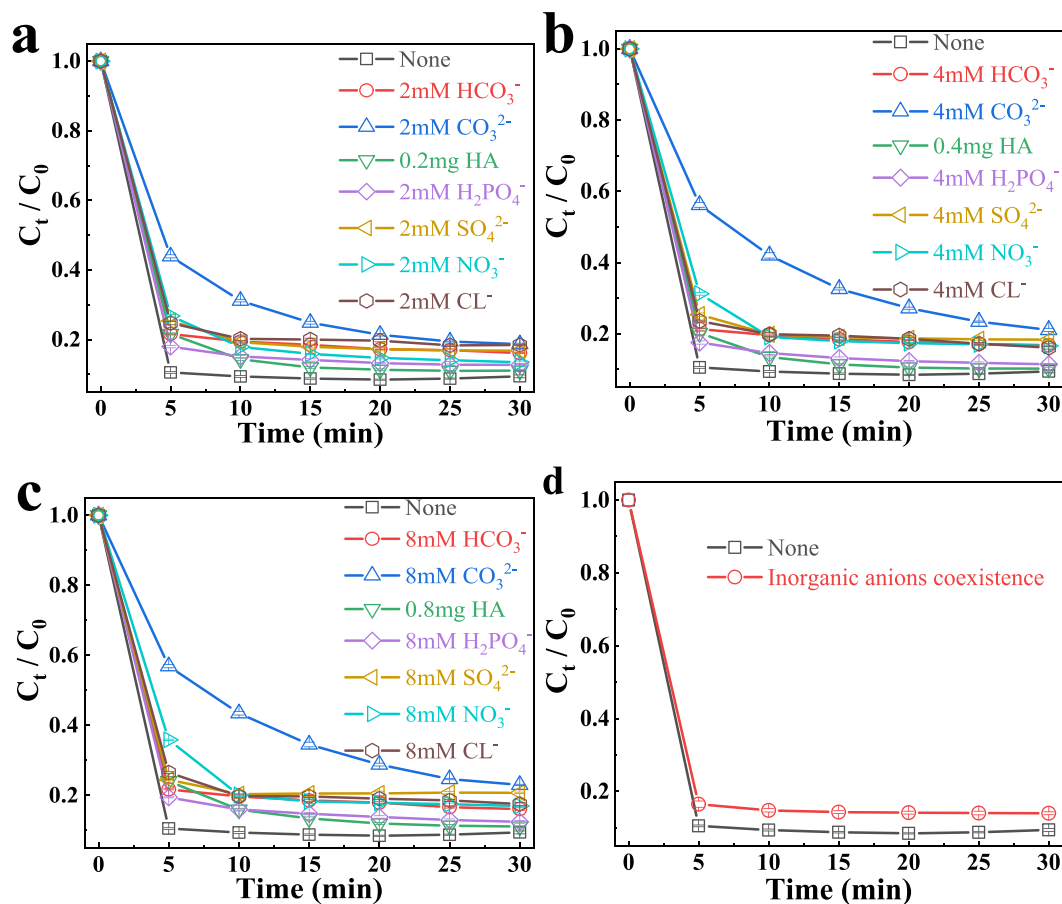


Fig. 11. (a – c) The degradation effect of FeCo – MOF on TC at different inorganic anions corresponding to different concentrations, (d) The degradation effect of FeCo – MOF on TC at coexistence of the inorganic anions.

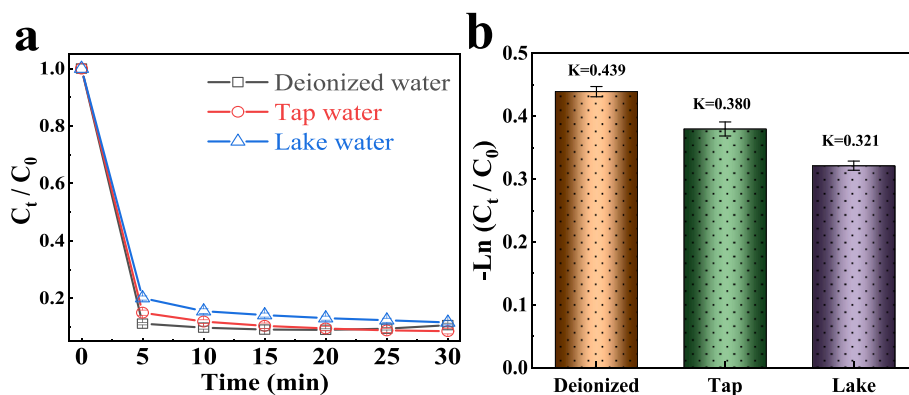


Fig. 12. (a) The degradation effect of FeCo – MOF on TC at different water bodies, (b) and the K value of FeCo – MOF/PMS/TC at different water bodies.

constant of TC in the lake water is only 0.321 min^{-1} . Thankfully, although tap water and lake water had some effect on the degradation of TC, the overall effect was satisfactory. It also shows that the catalytic system has superior degradation performance for TC in different water bodies.

In addition, other organic pollutants, including TC, methyl orange (MO) and methylene blue (MB), were degraded under the same experimental conditions. As shown in (Fig. 13a), The results clearly obvious that the catalytic system showed more rapid degradation of MO and MB.

The TC removal rate of the catalytic system is about 91 %, while the removal rate of MO and MB can reach about 100 % (Fig. 13b). The different removal rates achieved for different types of contaminants was ascribed to the effect of their substituents which determined the oxidation capacity in AOP (Wang et al., 2022). As $^1\text{O}_2$ and $\text{O}_2^{\bullet-}$ are the primary ROS in the FeCo – MOF/PMS system, they tend to react with electron – rich substances, such as the organics with electron donating groups (e.g. like $-\text{CH}_3$, $-\text{OH}$, $-\text{NH}_2$, and $-\text{NR}_2$), but have lower reactivities to substances with electron withdrawing groups (e.g. $-\text{NO}_2$).

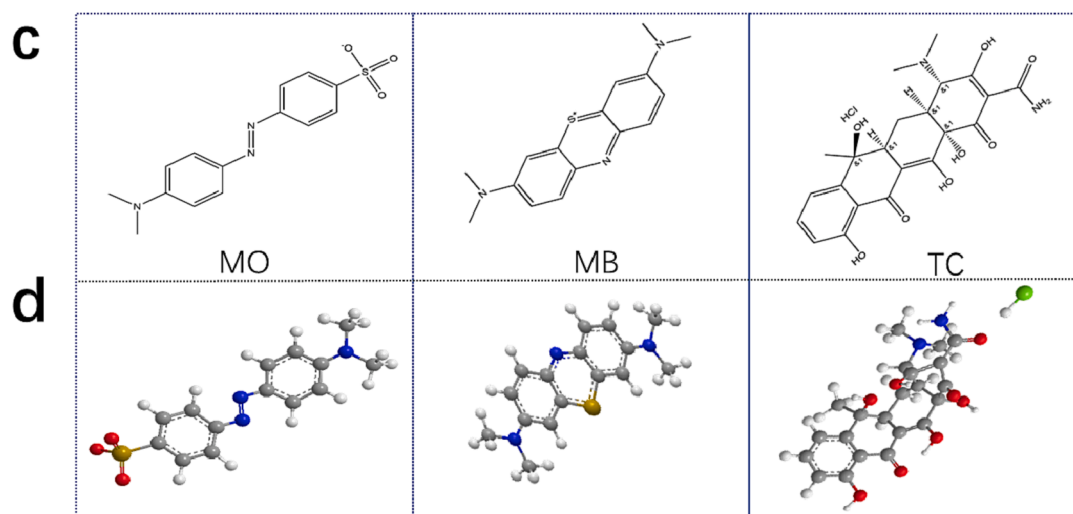
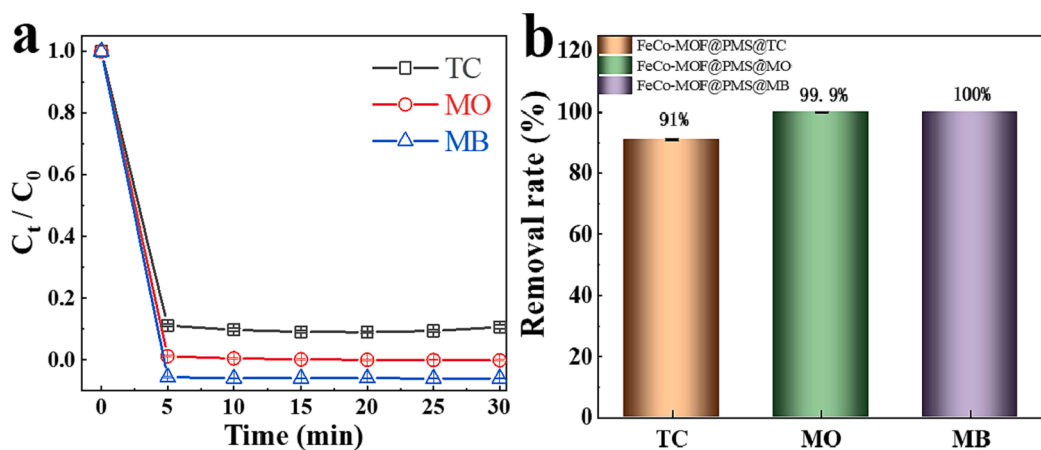


Fig. 13. The degradation curves of various contaminants (a), the corresponding removal rates (b), the Structural formulas and spatial ball and stick models for corresponding organic pollutants (c – d). Experimental condition: [contaminants]₀ = 20 mg/L, [PMS]₀ = 0.1 mM, [catalyst]₀ = 100 mg/L, pH ≈ 6, T ≈ 298 K.

(Li et al., 2022); (Xiao et al., 2016). As shown in Fig. 13c – d, the structures of MO, MB, TC all contain certain $-\text{CH}_3$, $-\text{OH}$, or $-\text{NH}_2$. This indicates that all three organic pollutants can be successfully degraded by the FeCo – MOF/PMS system. In addition, the degradation rate of TC is not as high as that of MO and MB, and the possible reason is that the relatively large molecular weight of TC, and the molecular structure is more complex.

4. Conclusions

FeCo – MOF had enhanced adsorption of TC. The adsorption data are well fitted by the pseudo – second – order kinetic model and Langmuir model, indicating the adsorption belongs to monolayer molecular adsorption and chemisorption. Negative gibbs free energy change, positive entropy change and positive enthalpy change proved that the adsorption had spontaneous endothermic property, and the enhancing temperature is benefit to the boosting of TC uptake. FeCo – MOF also can effectively active peroxymonosulfate for the TC degradation. For the TC degradation by the FeCo – MOF/PMS system, the higher temperature is better, the neutral pH is the best in the range of 2–12, and 1 mM/L is the best concentration of PMS in the range of 0.5–4 mM/L. The coexisting inorganic anions and small molecule acids slightly inhibited the catalytic performance of FeCo – MOF/PMS. Scavenger results show $\bullet\text{OH}$, $\text{SO}_4^{\bullet-}$, $\text{O}_2^{\bullet-}$ and $^1\text{O}_2$ all participate in the TC degradation. Generally, FeCo – MOF as an efficient adsorbent and catalyst had a potential application in water treatment applications.

Declaration of competing interest

The authors declare that they have no known competing financial interests or personal relationships that could have appeared to influence the work reported in this paper.

Acknowledgment

This work was supported by the National Natural Science Foundation of China (Grant No. 21767009) and Hubei Key Laboratory of Biologic Resources Protection and Utilization (Hubei Minzu University) (Grant No. KYPT012402).

Appendix A. Supplementary material

Supplementary data to this article can be found online at <https://doi.org/10.1016/j.arabjc.2023.105483>.

References

- Al–Mhyawi, S.R., Bader, D.M.D., Bajaber, M.A., Abd El Dayem, S.M., Ragab, A.H., Abd El–Rahem, K.A., Gado, M.A., Atia, B.M., Cheira, M.F., 2023. Zirconium oxide with graphene oxide anchoring for improved heavy metal ions adsorption: Isotherm and kinetic study. *J. Mater. Res. Technol.* 22, 3058–3074.
- Asif, M.B., Ji, B.X., Maqbool, T., Zhang, Z.H., 2021. Allogenic organic matter fouling alleviation in membrane distillation by peroxymonosulfate (PMS): Role of PMS concentration and activation temperature. *Desalination* 516, 115225.
- Azizollahi, N., Fatehizadeh, A., Pourzamani, H., Taheri, E., Aminabhavi, T.M., 2023. Degradation of 2,4–dichlorophenol via coupling zero valent iron and hydrodynamic cavitation for sulfite activation: A turbulence modeling. *J. Environ. Manage.* 332, 117295.
- Banerjee, A., Gokhale, R., Bhatnagar, S., Jog, J., Bhardwaj, M., Lefez, B., Hannover, B., Ogale, S., 2012. MOF derived porous carbon– Fe_3O_4 nanocomposite as a high performance, recyclable environmental superadsorbent. *J. Mater. Chem.* 22, 19694–19699.
- Bui, D.P., Nguyen, T.D., Vo, T.T.L., Cao, T.M., You, S.J., Pham, V.V., 2021. SnO_2 -x nanoparticles decorated on graphitic carbon nitride as S–scheme photocatalysts for activation of peroxymonosulfate. *ACS Appl. Nano Mater.* 4, 9333–9343.
- Chen, G.Y., He, S., Shi, G.B., et al., 2021. In-situ immobilization of ZIF-67 on wood aerogel for effective removal of tetracycline from water. *Chem. Eng. J.* 423, 130184.
- Chen, B., Li, Y., Du, Q., Pi, X., Wang, Y., Sun, Y., Wang, M., Zhang, Y., Chen, K., Zhu, J., 2022. Effective removal of tetracycline from water using copper alginate @ graphene oxide with in-situ grown MOF–525 composite: Synthesis, characterization and adsorption mechanisms. *Nanomaterials* 12, 2897.
- Chen, Y., Tang, J., Wang, S., Zhang, L., 2022. Facile preparation of a remarkable MOF adsorbent for Au(III) selective separation from wastewater: Adsorption, regeneration and mechanism. *J. Mol. Liq.* 349, 118137.
- Chen, L., Zuo, X., Zhou, L., Huang, Y., Yang, S., Cai, T., Ding, D., 2018. Efficient heterogeneous activation of peroxymonosulfate by facilely prepared Co/Fe bimetallic oxides: Kinetics and mechanism. *Chem. Eng. J.* 345, 364–374.
- Chen, L., Wang, H.F., Li, C., Xu, Q., 2020. Bimetallic metal–organic frameworks and their derivatives. *Chem. Sci.* 11, 5369–5403.
- Duan, X.G., Indrawirawan, S., Kang, J., Tian, W.J., Zhang, H.Y., Sun, H.Q., Wang, S.B., 2018. Temperature–dependent evolution of hydroxyl radicals from peroxymonosulfate activation over nitrogen–modified carbon nanotubes. *Sustain. Mater. Technol.* 18, e00082.
- El–Aswar, E.I., Ramadan, H., Elkik, H., Taha, A.G., 2022. A comprehensive review on preparation, functionalization and recent applications of nanofiber membranes in wastewater treatment. *J. Environ. Manage.* 301, 113908.
- ElMetwally, A.E., Goodarzi, F., Meier, K.K., Zahrani, E.M., Rayat, S., Kegnaes, S., Knecht, M.R., Bachas, L.G., 2021. $\text{Cu}_2\text{S}@\text{Bi}_2\text{S}_3$ double–shelled hollow cages as a nanocatalyst with substantial activity in peroxymonosulfate activation for atrazine degradation. *ACS Appl. Nano Mater.* 4, 12222–12234.
- Ge, K., Sun, S., Zhao, Y., Yang, K., Wang, S., Zhang, Z., Cao, J., Yang, Y., Zhang, Y., Pan, M., Zhu, L., 2021. Facile synthesis of two–dimensional iron/cobalt metal–organic framework for efficient oxygen evolution electrocatalysis. *Angew. Chem. Int. Edit.* 60, 12097–12102.
- Ghorbani, M., Sheibani, S., Abdizadeh, H., Golobostanfard, M.R., 2023. Modified $\text{BiFeO}_3/\text{rGO}$ nanocomposite by controlled synthesis to enhance adsorption and visible–light photocatalytic activity. *J. Mater. Res. Technol.* 22, 1250–1267.
- Gong, C., Chen, F., Yang, Q., Luo, K., Yao, F., Wang, S., Wang, X., Wu, J., Li, X., Wang, D., Zeng, G., 2017. Heterogeneous activation of peroxymonosulfate by Fe–Co layered doubled hydroxide for efficient catalytic degradation of Rhoadmine B. *Chem. Eng. J.* 321, 222–232.
- Habimana, F., Huo, Y., Jiang, S., Ji, S., 2016. Synthesis of europium metal–organic framework (Eu–MOF) and its performance in adsorptive desulfurization. *Adsorption* 22, 1147–1155.
- Huang, W.K., Jin, X.T., Li, Q.Y., Wang, Y.L., Huang, D., Fan, S.W., Yan, J.Y., Huang, Y.P., Astruc, D., Liu, X., 2023. Co_3O_4 Nanocubes for degradation of oxytetracycline in wastewater via peroxymonosulfate activation. *ACS Appl. Nano Mater.* 6, 12497–12506.
- Jiang, Y.C., Luo, M.F., Niu, Z.N., Xu, S.Y., Gao, Y., Gao, Y., Gao, W.J., Luo, J.J., Liu, R.L., 2023. In-situ growth of bimetallic FeCo–MOF on magnetic biochar for enhanced clearance of tetracycline and fruit preservation. *Chem. Eng. J.* 451, 138804.
- Khakbaz, F., Mirzaei, M., Mahani, M., 2022. Enhanced adsorption of crystal violet using Bi^{3+} –intercalated Cd–MOF: isotherm, kinetic and thermodynamic study. *Particul. Sci. Technol.* 40, 1004–1016.
- Lai, L., Yan, J., Li, J., Lai, B., 2018. Co/ Al_2O_3 –EPM as peroxymonosulfate activator for sulfamethoxazole removal: Performance, biotoxicity, degradation pathways and mechanism. *Chem. Eng. J.* 343, 676–688.
- Li, G., Cao, X., Meng, N., Huang, Y., Wang, X., Gao, Y., Li, X., Yang, T., Li, B., Zhang, Y., Lyu, X., Liang, Y., 2022. Fe_3O_4 supported on water caltrop–derived biochar toward peroxymonosulfate activation for urea degradation: the key role of sulfate radical. *Chem. Eng. J.* 433, 133595.
- Li, C.X., Chen, C.B., Wang, Y., Fu, X.Z., Cui, S., Lu, J.Y., Li, J., Liu, H.Q., Li, W.W., Lau, T. C., 2019. Insights on the pH–dependent roles of peroxymonosulfate and chlorine ions in phenol oxidative transformation. *Chem. Eng. J.* 362, 570–575.
- Li, L., Liu, X.L., Geng, H.Y., Hu, B., Song, G.W., Xu, Z.S., 2013. A MOF/graphite oxide hybrid (MOF: HKUST–1) material for the adsorption of methylene blue from aqueous solution. *J. Mater. Chem. A* 1, 10292–10299.
- Li, H., Zhang, J., Yao, Y., Miao, X., Chen, J., Tang, J., 2019. Nanoporous bimetallic metal–organic framework (FeCo–BDC) as a novel catalyst for efficient removal of organic contaminants. *Environ. Pollut.* 255, 113337.
- Li, H., Yao, Y., Chen, J., Wang, C., Huang, J., Du, J., Xu, S., Tang, J., Zhao, H., Huang, M., 2021. Heterogeneous activation of peroxymonosulfate by bimetallic MOFs for efficient degradation of phenanthrene: Synthesis, performance, kinetics, and mechanisms. *Sep. Purif. Technol.* 259, 118217.
- Liu, T., Cui, K.P., Chen, Y.H., Li, C.X., Cui, M.S., Yao, H.J., Chen, Y.W., Wang, S.P., 2021. Removal of chlorophenols in the aquatic environment by activation of peroxymonosulfate with nMnO_x @Biochar hybrid composites: Performance and mechanism. *Chemosphere* 283, 131188.
- Liu, F., Li, W., Wu, D., Tian, T., Wu, J.F., Dong, Z.M., Zhao, G.C., 2020. New insight into the mechanism of peroxymonosulfate activation by nanoscaled lead–based spinel for organic matters degradation: A singlet oxygen–dominated oxidation process. *J. Colloid Interface Sci.* 572, 318–327.
- Liu, R.L., Liu, Y., Zhou, X.Y., Zhang, Z.Q., Zhang, J., Dang, F.Q., 2014. Biomass–derived highly porous functional carbon fabricated by using a free–standing template for efficient removal of methylene blue. *Bioresour. Technol.* 154, 138–147.
- Liu, S., Qiu, Y., Liu, Y., Zhang, W., Dai, Z., Srivastava, D., Kumar, A., Pan, Y., Liu, J., 2022. Recent advances in bimetallic metal–organic frameworks (BMOFs): synthesis, applications and challenges. *New J. Chem.* 46, 13818–13837.
- Liu, R.L., Yu, P., Luo, Z.M., Bai, X.F., Li, X.Q., Fu, Q., 2017. Single–helix carbon microcoils prepared via Fe(III)–osmotically induced shape transformation of zucchini (Cucurbita pepo L.) for enhanced adsorption and antibacterial activities. *Chem. Eng. J.* 315, 437–447.
- Lou, X., Fang, C., Geng, Z., Jin, Y., Xiao, D., Wang, Z., Liu, J., Guo, Y., 2017. Significantly enhanced base activation of peroxymonosulfate by polyphosphates: Kinetics and mechanism. *Chemosphere* 173, 529–534.

- Lou, X.Y., Guo, Y.G., Xiao, D.X., Wang, Z.H., Lu, S.Y., Liu, J.S., 2013. Rapid dye degradation with reactive oxidants generated by chloride-induced peroxymonosulfate activation. *Environ. Sci. Pollut. r.* 20, 6317–6323.
- Luo, J., Luo, X., Gan, Y., Xu, X., Xu, B., Liu, Z., Ding, C., Cui, Y., Sun, C., 2023. Advantages of Bimetallic Organic Frameworks in the Adsorption, Catalysis and Detection for Water Contaminants. *Nanomaterials* 13, 2194.
- Masoomi, M.Y., Morsali, A., Dhakshinamoorthy, A., Garcia, H., 2019. Mixed-metal MOFs: Unique opportunities in metal-organic framework (MOF) functionality and design. *Angew. Chem. Int. Edit.* 58, 15188–15205.
- Pan, C., Fu, L., Ding, Y., Peng, X., Mao, Q., 2020. Homogeneous catalytic activation of peroxymonosulfate and heterogeneous reductive regeneration of Co²⁺ by MoS₂: The pivotal role of pH. *Sci. Total Environ.* 712, 136447.
- Pang, Y., Ruan, Y., Feng, Y., Diaio, Z., Shih, K., Hou, L.A., Chen, D., Kong, L., 2019. Ultrasound assisted zero valent iron corrosion for peroxymonosulfate activation for Rhodamine-B degradation. *Chemosphere* 228, 412–417.
- Qin, W., Fang, G., Wang, Y., Zhou, D., 2018. Mechanistic understanding of polychlorinated biphenyls degradation by peroxymonosulfate activated with CuFe₂O₄ nanoparticles: Key role of superoxide radicals. *Chem. Eng. J.* 348, 526–534.
- Rao, Y., Zhang, Y., Fan, J., Wei, G., Wang, D., Han, F., Huang, Y., Croue, J.P., 2022. Enhanced peroxymonosulfate activation by Cu-doped LaFeO₃ with rich oxygen vacancies: Compound-specific mechanisms. *Chem. Eng. J.* 435, 134882.
- Samy, M., Gar Alalm, M., Khalil, M.N., Ezeldan, E., El-Dissouky, A., Nasr, M., Tawfik, A., 2023. Treatment of hazardous landfill leachate containing 1,4 dioxane by biochar-based photocatalysts in a solar photo-oxidation reactor. *J. Environ. Manage.* 332, 117402.
- Sanati, S., Abazari, R., Albero, J., Morsali, A., Garcia, H., Liang, Z., Zou, R., 2021. Metal-organic framework derived bimetallic materials for electrochemical energy storage. *Angew. Chem. Int. Edit.* 60, 11048–11067.
- Sanati, S., Morsali, A., Garcia, H., 2022. First-row transition metal-based materials derived from bimetallic metal-organic frameworks as highly efficient electrocatalysts for electrochemical water splitting. *Energ. Environ. Sci.* 15, 3119–3151.
- Scaria, J., Anupama, K.V., Nidheesh, P.V., 2021. Tetracyclines in the environment: An overview on the occurrence, fate, toxicity, detection, removal methods, and sludge management. *Sci. Total Environ.* 771, 145291.
- Shi, Y., Yang, A.F., Cao, C.S., Zhao, B., 2019. Applications of MOFs: Recent advances in photocatalytic hydrogen production from water. *Coord. Chem. Rev.* 390, 50–75.
- Tan, J., Xu, C., Zhang, X., Huang, Y., 2022. MOFs-derived defect carbon encapsulated magnetic metallic Co nanoparticles capable of efficiently activating PMS to rapidly degrade dyes. *Sep. Purif. Technol.* 289, 120812.
- Trawiński, J., Wronski, M., Skibiński, R., 2022. Efficient removal of anti-HIV drug – maraviroc from natural water by peroxymonosulfate and TiO₂ photocatalytic oxidation: Kinetic studies and identification of transformation products. *J. Environ. Manage.* 319, 115735.
- Valadi, F.M., Shahsavari, S., Akbarzadeh, E., Gholami, M.R., 2022. Preparation of new MOF–808/chitosan composite for Cr(VI) adsorption from aqueous solution: Experimental and DFT study. *Carbohydr. Polym.* 288, 119383.
- Vinayagam, R., Kandati, S., Murugesan, G., Goveas, L.C., Baliga, A., Pai, S.D., Varadavenkatesan, T., Kaviyarasu, K., Selvaraj, R., 2023. Bioinspiration synthesis of hydroxyapatite nanoparticles using eggshells as a calcium source: Evaluation of Congo red dye adsorption potential. *J. Mater. Res. Technol.* 22, 169–180.
- Wang, Y., Cao, D., Liu, M., Zhao, X., 2017. Insights into heterogeneous catalytic activation of peroxymonosulfate by Pd/g-C₃N₄: The role of superoxide radical and singlet oxygen. *Catal. Commun.* 102, 85–88.
- Wang, J.G., Fan, S.Y., Li, X.Y., Wang, P.L., Niu, Z.D., Yang, J., Tao, Y.Y., Chen, A.C., 2022a. Tailoring the Mn–O Covalency and Surface Oxygen Defects of Ferrite Nanostructures for Peroxymonosulfate Activation and Norfloxacin Degradation. *Acs Appl. Nano Mater.*, 5.
- Wang, H., Guo, W., Si, Q., Liu, B., Zhao, Q., Luo, H., Ren, N., 2021. Non-covalent doping of carbon nitride with biochar: Boosted peroxymonosulfate activation performance and unexpected singlet oxygen evolution mechanism. *Chem. Eng. J.* 418, 129504.
- Wang, Z., Jia, W., Jiang, M., Chen, C., Li, Y., 2016. One-step accurate synthesis of shell controllable CoFe₂O₄ hollow microspheres as high-performance electrode materials in supercapacitor. *Nano Res.* 9, 2026–2033.
- Wang, Q., Lu, J., Jiang, Y., Yang, S., Yang, Y., Wang, Z., 2022. FeCo bimetallic metal organic framework nanosheets as peroxymonosulfate activator for selective oxidation of organic pollutants. *Chem. Eng. J.* 443, 136483.
- Wang, S., Wang, J., 2018. Radiation-induced degradation of sulfamethoxazole in the presence of various inorganic anions. *Chem. Eng. J.* 351, 688–696.
- Wang, J., Wang, S., 2021. Effect of inorganic anions on the performance of advanced oxidation processes for degradation of organic contaminants. *Chem. Eng. J.* 411, 128392.
- Xia, T., Lin, Y., Li, W., Ju, M., 2021. Photocatalytic degradation of organic pollutants by MOFs based materials: A review. *Chinese Chem. Lett.* 32, 2975–2984.
- Xiao, J., Xie, Y., Han, Q., Cao, H., Wang, Y., Nawaz, F., Duan, F., 2016. Superoxide radical-mediated photocatalytic oxidation of phenolic compounds over Ag⁺/TiO₂: Influence of electron donating and withdrawing substituents. *J. Hazard. Mater.* 304, 126–133.
- Xu, L.J., Duan, L., Pan, Y.W., Zhang, Y., Qi, L.Y., Mei, X., Qiao, W.C., Gan, L., 2022. Mechanistic study of cobalt and iron based Prussian blue analogues to activate peroxymonosulfate for efficient diclofenac degradation. *Sep. Purif. Technol.* 303, 122137.
- Yan, Y.T., Zhang, H.Y., Wang, W., Li, W.C., Ren, Y.P., Li, X.F., 2021. Synthesis of Fe⁰/Fe₃O₄@porous carbon through a facile heat treatment of iron-containing candle soots for peroxymonosulfate activation and efficient degradation of sulfamethoxazole. *J. Hazard. Mater.* 411, 124952.
- Yang, S.S., Zhu, R., Li, C.Q., Zhang, X.W., Zheng, S.L., Sun, Z.M., 2023. Enhanced peroxymonosulfate activation for antibiotics degradation over FeOOH regulated by kaolinite with pleiotropic effects. *Sep. Purif. Technol.* 324, 124552.
- Yao, Y., Cai, Y., Lu, F., Wei, F., Wang, X., Wang, S., 2014. Magnetic recoverable MnFe₂O₄ and MnFe₂O₄-graphene hybrid as heterogeneous catalysts of peroxymonosulfate activation for efficient degradation of aqueous organic pollutants. *J. Hazard. Mater.* 270, 61–70.
- Yu, Y., Li, N., Wang, C.B., Cheng, Z.J., Yan, B.B., Chen, G.Y., Hou, L.A., Wang, S.B., 2022. Iron cobalt and nitrogen co-doped carbonized wood sponge for peroxymonosulfate activation: Performance and internal temperature-dependent mechanism. *J. Colloid Interface Sci.* 619, 267–279.
- Yuan, G.E., Qin, Y., Feng, M., Ru, X., Zhang, X., 2021. Activation of peroxymonosulfate by natural molybdenite for dye degradation: Identification of reactive species and catalytic mechanism. *Environ. Technol. Inno.* 22, 101403.
- Zhang, C., Ai, L., Jiang, J., 2015. Graphene hybridized photoactive iron terephthalate with enhanced photocatalytic activity for the degradation of Rhodamine B under visible light. *Ind. Eng. Chem. Res.* 54, 153–163.
- Zhang, X.K., Liu, J., Zhang, H.Z., et al., 2023. Uncovering the pathway of peroxymonosulfate activation over Co_{0.5}Zn_{0.5}O nanosheets for singlet oxygen generation: Performance and membrane application. *Appl. Catal. B-Environ.* 327, 122429.
- Zhang, R., Sun, P., Boyer, T.H., Zhao, L., Huang, C.H., 2015. Degradation of pharmaceuticals and metabolite in synthetic human urine by UV, UV/H₂O₂, and UV/PDS. *Environ. Sci. Technol.* 49, 3056–3066.
- Zhang, G.Q., Zhu, X.Y., Yu, M.Q., Yang, F.L., 2023. Electrochemical activation of peroxymonosulfate using chlorella biochar modified flat ceramic membrane cathode for berberine removal: Role of superoxide radical and mechanism insight. *Sep. Purif. Technol.* 318, 124002.
- Zhao, L., Dong, B., Li, S., Zhou, L., Lai, L., Wang, Z., Zhao, S., Han, M., Gao, K., Lu, M., Xie, X., Chen, B., Liu, Z., Wang, X., Zhang, H., Li, H., Liu, J., Zhang, H., Huang, X., Huang, W., 2017. Interdiffusion reaction-assisted hybridization of two-dimensional metal-organic frameworks and Ti₃C₂T_x nanosheets for electrocatalytic oxygen evolution. *ACS Nano* 11, 5800–5807.
- Zhao, X., Huang, Y., Liu, X., Yan, J., Ding, L., Zong, M., Liu, P., Li, T., 2022. Core-shell CoFe₂O₄@C nanoparticles coupled with rGO for strong wideband microwave absorption. *J. Colloid Interface Sci.* 607, 192–202.
- Zhao, C.H., Shao, B.B., Yan, M., Liu, Z.F., Liang, Q.H., He, Q.Y., Wu, T., Liu, Y., Pan, Y., Huang, J., Wang, J.J., Liang, J., Tang, L., 2021. Activation of peroxymonosulfate by biochar-based catalysts and applications in the degradation of organic contaminants: A review. *Chem. Eng. J.* 416, 128829.
- Zhong, Q., Liu, J., Wang, J.T., et al., 2022. Efficient degradation of organic pollutants by activated peroxymonosulfate over TiO₂@C decorated Mg-Fe layered double oxides: Degradation pathways and mechanism. *Chemosphere* 300, 134564.
- Zhou, X.Y., Liu, Y.Y., Miao, Y.Q., He, W.W., Pan, Y.A., Li, A.J., Qin, J.H., Li, H.S., Yin, R. L., Qiu, R.L., 2023. Coupled radical and nonradical activation of peroxymonosulfate by the piezo-photocatalytic effect of alpha-SnWO₄/ZnO heterojunction to boost the degradation and detoxification of carbamazepine. *Sep. Purif. Technol.* 323, 124410.
- Zhu, J., Zhu, Y., Zhou, W., 2022. Cu-doped Ni-LDH with abundant oxygen vacancies for enhanced methyl 4-hydroxybenzoate degradation via peroxymonosulfate activation: key role of superoxide radicals. *J. Colloid Interface Sci.* 610, 504–517.